Wintertime phytoplankton bloom in the subarctic Pacific supported by continental margin iron

Phoebe J. Lam,[1,2,3] James K. B. Bishop,[1] Cara C. Henning,[4] Matthew A. Marcus,[5] Glenn A. Waychunas,[1] and Inez Y. Fung[4]

[1] Heightened biological activity was observed in February 1996 in the high-nutrient low-chlorophyll (HNLC) subarctic North Pacific Ocean, a region that is thought to be iron-limited. Here we provide evidence supporting the hypothesis that Ocean Station Papa (OSP) in the subarctic Pacific received a lateral supply of particulate iron from the continental margin off the Aleutian Islands in the winter, coincident with the observed biological bloom. Synchrotron X-ray analysis was used to describe the physical form, chemistry, and depth distributions of iron in size fractionated particulate matter samples. The analysis reveals that discrete micron-sized iron-rich hot spots are ubiquitous in the upper 200 m at OSP, more than 900 km from the closest coast. The specifics of the chemistry and depth profiles of the Fe hot spots trace them to the continental margins. We thus hypothesize that iron hot spots are a marker for the delivery of iron from the continental margin. We confirm the delivery of continental margin iron to the open ocean using an ocean general circulation model with an iron-like tracer source at the continental margin. We suggest that iron from the continental margin stimulated a wintertime phytoplankton bloom, partially relieving the HNLC condition.

Citation: Lam, P. J., J. K. B. Bishop, C. C. Henning, M. A. Marcus, G. A. Waychunas, and I. Y. Fung (2006), Wintertime phytoplankton bloom in the subarctic Pacific supported by continental margin iron, *Global Biogeochem. Cycles*, *20*, GB1006, doi:10.1029/2005GB002557.

1. Introduction

[2] Iron controls primary productivity in many regions of the world's oceans [*Martin et al.*, 1994; *Coale et al.*, 1996; *Boyd et al.*, 2000; *Tsuda et al.*, 2003; *Boyd et al.*, 2004; *Coale et al.*, 2004]. There have been several models of the cycling of iron in the oceans [*Lefevre and Watson*, 1999; *Archer and Johnson*, 2000; *Fung et al.*, 2000; *Parekh et al.*, 2004], and parameterizations of the iron cycle are now being incorporated into global scale ecosystem models [*Aumont et al.*, 2003; *Gregg et al.*, 2003; *Moore et al.*, 2004]. Most global scale modeling studies until now have focused on the importance of aeolian dust delivery as the primary external iron source to the open ocean. However, it has been speculated that iron from shelf sediments is responsible for the elevated chlorophyll concentrations observed downstream of islands and shelves in high-

nutrient low-chlorophyll (HNLC) waters of the equatorial Pacific and the Atlantic and Indian sectors of the Southern Ocean [*Perissinotto et al.*, 1992; *Martin et al.*, 1994; *de Baar et al.*, 1995; *Lindley and Barber*, 1998; *Moore and Abbott*, 2000; *Atkinson et al.*, 2001; *Blain et al.*, 2001]. Farther north, continental margin sediments have been shown to be important sources of iron off the California coast [*Johnson et al.*, 1999, 2003]. Recent studies have shown that this iron may be transported offshore into the oligotrophic North Pacific gyre [*Johnson et al.*, 2003] and that iron from the continental margin is a significant term in the global iron budget [*Elrod et al.*, 2004]. The continental margin surrounding the high-latitude North Pacific has thus far escaped scrutiny. Primary production in the subarctic Pacific, the third major iron-limited HNLC region, is still thought to be primarily controlled by dust inputs of iron [*Martin*, 1991; *Boyd et al.*, 1998; *Bishop et al.*, 2002].

[3] In this study, we investigate samples collected from Ocean Station Papa (OSP) in the HNLC subarctic Pacific in winter and spring. We present novel Fe data from these samples that strongly suggest that the HNLC subarctic Pacific receives iron from the continental margin, and that this iron stimulated a wintertime bloom at OSP, more than 900 km from the closest coast.

2. Methods

[4] We collected depth profiles (up to 12 samples between the surface and 1000 m) of large volume (~10,000 L) size-

---

[1]Earth Sciences Division, Lawrence Berkeley National Laboratory, Berkeley, California, USA.
[2]Also at Department of Earth and Planetary Science, University of California, Berkeley, Berkeley, California, USA.
[3]Now at Department of Marine Chemistry and Geochemistry, Woods Hole Oceanographic Institution, Woods Hole, Massachusetts, USA.
[4]Berkeley Atmospheric Sciences Center, University of California, Berkeley, Berkeley, California, USA.
[5]Advanced Light Source, Lawrence Berkeley National Laboratory, Berkeley, California, USA.

Table 1. ICPMS and XRF Fe Concentrations in the Water Column From Subarctic Pacific Samples[a]

Station	Depth, m	Potential Density (σ_θ)	1- to 53-μm Size Fraction, pM				>53-μm Size Fraction, pM			
			XRF HotFe	XRF DetFe	XRF TotFe	ICPMS Fe	XRF HotFe	XRF DetFe	XRF TotFe	ICPMS Fe
FebOSP	22	25.72	46	132	171	354	18	54	70	136
FebOSP	46	25.72	55	144	180	266	26	71	76	320
FebOSP	71	25.73	29	65	67	197	21 (2)	30 (27)	101 (35)	103
FebOSP	95	25.73	34 (23)	65 (12)	94 (35)	300	29	71	80	221
FebOSP	144	26.54	50	278	280	217	11 (1)	27 (4)	31 (6)	24
FebOSP	193	26.72	49	238	240	328	10	29	33	41
FebOSP	315	26.87	17	73	83	163	2	10	13	15
FebOSP	462	27.00	27	107	118	206				121
FebOSP	658	27.17	17	171	172	198	1	3	3	14
FebOSP	805	27.26	13	166	167	166				17
FebOSP	903	27.30				391	2	8	11	15
FebP16	89	25.38				261	50	94	103	35
FebP16	138	26.30				1555	37	66	71	67
FebP4	62	25.65				19605	1561	1689	1690	2476
FebP4	86	26.09				38112	763	802	803	2094
FebP4	134	26.26	64269	64257	64261	46186	1880	1924	1924	2301
MayOSP	12	25.58				86	17	47	67	43
MayOSP	36	25.60				86	117	191	207	84
MayOSP	135	26.46				159	34 (10)	58 (5)	65 (1)	25
MayOSP	552	27.11				231	4	12	15	5

[a]Inductively coupled plasma mass spectrometry, ICPMS; X-ray fluorescence, XRF. FebOSP and MayOSP samples were collected in February and May 1996, respectively. FebP16 and FebP4 samples were collected in February 1997. Blank cells denote samples that were not run. When more than one map was collected for a sample, the mean value is indicated, with the standard deviation in parentheses (sd).

fractionated particulate samples using the Multiple Unit Large Volume in situ Filtration System (MULVFS) [*Bishop et al.*, 1985]. Samples were collected along "Line P," a transect from the British Columbian coast to the open ocean in the northeast HNLC subarctic Pacific, in winter 1996 and 1997, spring 1996, and summer 1996, as well as from the HNLC Southern Ocean (55°S, 172°W) in January/February 2002. Size fractions are >53 μm and 1−53 μm for the subarctic Pacific samples, and >51 μm and 1−51 μm for the Southern Ocean samples. We focus primarily on subarctic Pacific samples collected in February and May 1996 from Ocean Station Papa (OSP, 50°N, 145°W) and from Stations P16 (49°58.2′N, 134°40.0′W) and P4 (48°38.0′N, 126°40.0′W) in February 1997.

[5] All size-fractionated particulate samples were analyzed using inductively coupled plasma mass spectrometry (ICP-MS), and a subset of the samples were analyzed using synchrotron micro-X-ray fluorescence (μ-XRF), micro-extended X-ray absorption fine structure (μ-EXAFS) spectroscopy, and scanning transmission X-ray microscopy (STXM). All synchrotron data were collected at the Advanced Light Source at Lawrence Berkeley National Lab in Berkeley, California. The μ-XRF and μ-EXAFS were collected at the microprobe beamline 10.3.2 [*Marcus et al.*, 2004], and STXM data was collected at beamline 11.0.2 [*Kilcoyne et al.*, 2003].

[6] The ICP-MS provides bulk chemical properties of the particles. Here we use ICP-MS determined acid-leachable Fe, Mn, and Ca concentrations from depth profiles along Line P (OSP and Stations P16 and P4).

[7] The μ-XRF and STXM map the spatial distribution of elements at resolutions of 7 μm and 40 nm, respectively. We used μ-XRF to map Ca, Ti, Cr, Mn, and Fe. We quantify Fe counts from μ-XRF maps of depth profiles of large and small size-fractionated particulate samples from OSP col-

lected in February and May 1996, and from the Southern Ocean collected in January 2002. To derive the concentration of XRF Fe in the water column, we first corrected XRF Fe maps for background and filter Fe and assumed the remaining Fe counts ("corrected-Fe") to be from the sample. The detection limit of XRF Fe per pixel (2.7×10^{-10} μmol Fe/pixel) was determined as 3 times the standard deviation of the corrected-Fe pixels of each mesh blank. "Hot spots" were defined to be pixels with Fe above the hot spot threshold, chosen to be 10 times the detection limit, which amounts to 2.7×10^{-9} μmol Fe/pixel or 6.8×10^{-8} μmol Fe/μm^2. For each XRF map, we defined "total XRF Fe" as the sum of corrected-Fe counts and "XRF detectable Fe" and "hot spot Fe" as the sum of corrected-Fe counts greater than the detection limit and hot spot threshold, respectively. All forms of XRF Fe were corrected for sample heterogeneity on the filter using Ca concentrations determined by both XRF and ICP-MS, and finally divided by the volume filtered through the equivalent filter area of the map (∼100 mL; auxiliary material[1] Table ts01) to obtain the concentration of XRF Fe in the water column (Table 1).

[8] We selected a sample collected at 46 m from within the mixed layer in February 1996 from OSP and used Fe K-edge μ-EXAFS to provide information on the local bonding environments of particulate Fe, and used STXM to obtain high-resolution Fe images. Further details of data collection and analysis are described in the auxiliary material.

3. Results

3.1. Biological Observations at OSP

[9] Surprisingly, >53-μm samples obtained from the 110-m-deep wintertime mixed layer at OSP in February

---

[1]Auxiliary material is available at ftp://ftp.agu.org/apend/gb/2005GB002557.

1996 were dominated by large chain forming diatoms (*Fragilariopsis* sp. and *Chaetoceros* sp.) and accompanied by abundant large (hundreds of microns) aggregates of smaller particles. These aggregates were loaded with $CaCO_3$ coccoliths, which derived from the remarkably high abundance of the coccolithophore *Emiliania huxleyi* in the 1- to 53-μm fraction at this time (0.27 μM $CaCO_3$ in February 1996 compared to only 0.02 μM in May 1996 and 0.17 μM in August 1996); *E. huxleyi* was negligible in May and August. *Fragilariopsis* sp. and *Chaetoceros* sp. are diatom species that have dominated subpolar phytoplankton assemblages after iron addition experiments [*Boyd et al.*, 2000; *Tsuda et al.*, 2003]. Such an unusual assemblage in an HNLC region is consistent with a recent supply of bioavailable iron.

3.2. Fe Hot Spots in Marine Particulates at OSP

[10] μ-XRF analysis of >53-μm mixed layer samples collected in February and May 1996 at OSP showed that iron was distributed as discrete pixels of hot spots dispersed in the aggregates (Figures 1a and 2a). The iron distribution was in stark contrast with calcium distributions, which showed micron-sized $CaCO_3$ coccoliths evenly spread throughout the aggregates (Figures 1b and 2b). The calcium maps were thereafter used to locate aggregates. There were few Fe hot spots not associated with aggregates. Overlaying the Fe and Ca maps show that iron hot spots were prevalent in aggregates throughout the water column in both February (Figure 1) and May (Figure 2). The observation of hot spots within biological aggregates gives us confidence that the hot spots are not from contamination. A high concentration of hot spot-Fe in the 1- to 53-μm samples (Table 1) confirmed that this small size fraction was the most likely source of the aggregate hot spots in the >53-μm samples. We postulate that the Fe hot spots are discrete, micronscale Fe-rich particles suspended in the water column. These small particles are passively captured by aggregating biological particles and are thus transferred to the large size class (>53 μm), where they are observed within aggregates.

3.3. Concentrations of Hot Spot Fe in the Subarctic Pacific

[11] Concentrations of all forms of iron (XRF hot spot Fe, XRF detectable Fe, total XRF Fe, and ICP-MS Fe) in both size fractions increase eastward toward the shore (Figure 3). The concentration of hot spot Fe in the upper 200 m at OSP in February 1996 ranged from 29 to 55 pM in 1- to 53-μm samples, and from 10 to 29 pM in >53-μm samples (Figures 3a and 3b and Table 1). In the 1- to 53-μm size fraction, the hot spots accounted for 20−36% of total XRF Fe and 11−23% of acid-leachable ICP-MS Fe. In the >53-μm size fraction, this amounted to 21−35% of total XRF Fe and 8−46% of ICP-MS Fe (Table 1). The detection of hot spot Fe is unequivocal since the hot spot threshold is significantly above the detection limit. Total XRF Fe is generally within a factor of 2 of acid-leachable Fe determined by ICP-MS (Figures 3a and 3b and Table 1). The differences between XRF- and ICP-MS-determined Fe concentrations are likely due to the factor of ∼1000 differences in the filter area subsampled for each measurement. The hot

spots were thus a significant, though not dominant, fraction of the total particulate iron. The balance of the particulate iron was spread more evenly throughout the sample, but was too diffuse to characterize with our method. The concentrated nature of the hot spots, however, made them ideal subjects for investigation at the microprobe beamline.

3.4. Size of Fe Hot Spots

[12] Since the ALS beamline 10.3.2 could not resolve anything smaller than 7 μm, we assumed each hot spot was a single spherical iron-rich particle, and calculated the expected size of a typical Fe hot spot (9×10^{-9} μmol Fe) for different potential compositions. An iron hydroxide (FeOOH) particle with density = 3.8 g/cm^3 would have a diameter of 0.7 μm. A generic Fe-silicate (5% Fe) with density = 3 g/cm^3 would have a diameter of 1.9 μm. We used a STXM with a 40-nm resolution to confirm the size of the Fe hot spots (Figure 4). The seven Fe hot spots imaged by STXM had a mean diameter of 1.7 μm and ranged between 0.8 and 3 μm.

3.5. Chemical Speciation of Fe Hot Spots

[13] EXAFS analysis of hot spots provided insight into their chemical speciation. EXAFS data of an iron hot spot ("Decspot 1") from a mixed layer (46 m) sample from OSP was well fit with a linear combination of iron hydroxide (63% goethite) and amorphous iron oxyhydroxide (37% ferrihydrite) (Figure 5). Other hot spots were not well fit with our limited reference compounds, indicating a more complex composition. Fits using the ab initio EXAFS simulation program FEFF [*Ankudinov et al.*, 1998] confirmed that the hot spots were heterogeneous, as each hot spot had different nearest neighbor identities and distances (Table 2). First shell Fe-O distances ranged from 1.96 to 2.16 Å and 1.89 to 2.04 Å for hot spots in the >53-μm and 1- to 53-μm size fractions, respectively. Second shell Fe-Fe distances ranged from 2.97 to 3.39 Å and 2.97 to 3.46 Å in the >53-μm and 1- to 53-μm size fractions, respectively. Second shell Fe-Si distances ranged from 3.18 to 3.51 Å in the >53-μm size fraction and was 3.16 Å in the 1- to 53-μm size fraction. The wide range in nearest neighbor characteristics show that the hot spots in both the small and large particulates are very different from one another and have a heterogeneous source, and suggests that the hot spots did not precipitate locally from a common source. The relatively strong second shell signal in all hot spots is inconsistent with carbon as an electron backscatterer, arguing against an organically bound Fe. Eight out of nine hot spots had Fe as a significant second shell electron backscatterer (Table 2). Three of these also had minor contributions to the fit from Si, with Fe-Si distances ranging from 3.16 to 3.51 Å. A single hot spot ("Julspot 1") was best fit with Si as a sole second shell electron backscatterer (Table 2).

4. Discussion

4.1. Origin of Fe Hot Spots

[14] There are three sources of iron to the open ocean: atmospheric dust deposition, lateral transport from the continental margin, and upwelling from below [*Fung et*
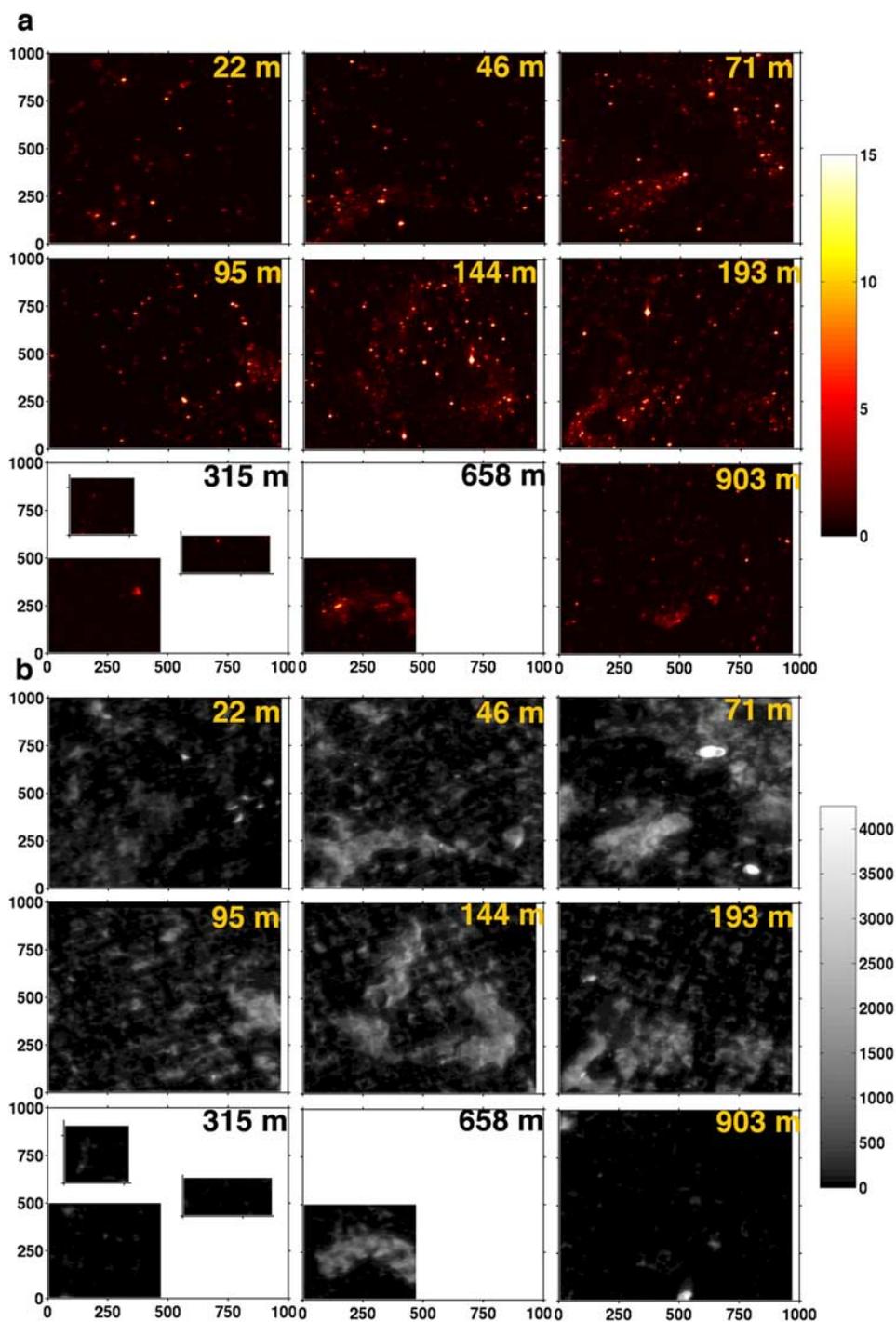
Figure 1. X-ray fluorescence (XRF) maps of >53-μm marine aggregates collected in February 1996 from Ocean Station Papa (OSP). (a) Depth profile of corrected FeKα maps; (b) Depth profile of corrected CaKα maps of same samples. FeKα maps show Fe hot spot distribution. CaKα maps show aggregate locations. Color bars are in μmol (Fe or Ca) × 10^9/pixel. Images are forced to the same scale for comparison. The pixel size was 5 μm.
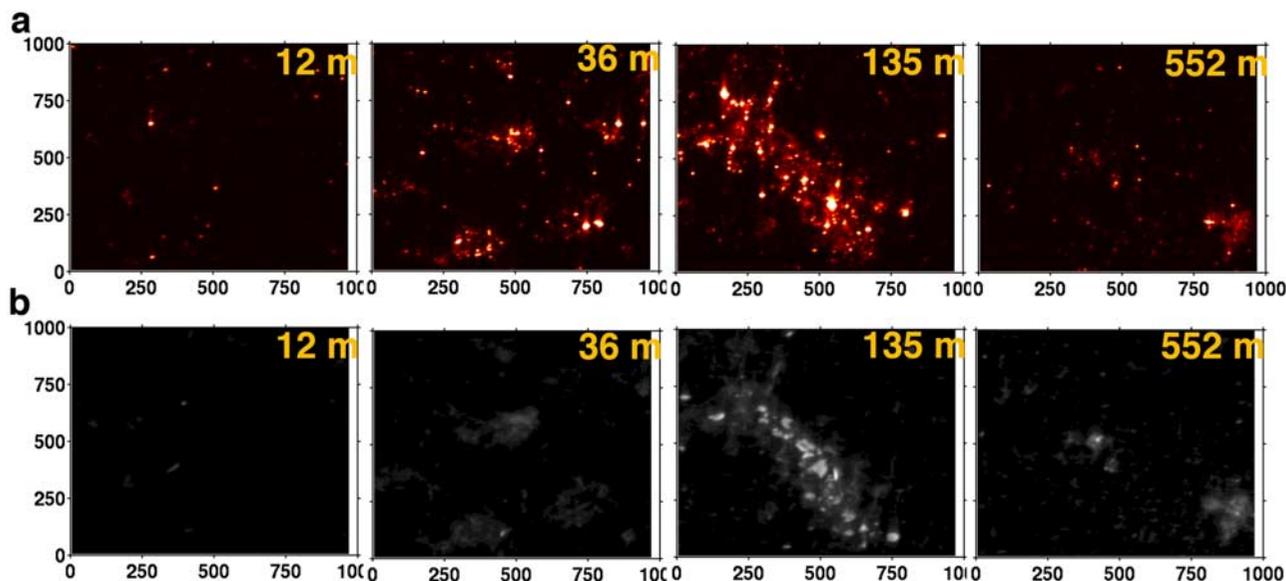
Figure 2. XRF maps of >53-μm marine aggregates collected in May 1996 from OSP. (a) Depth profile of corrected FeKα maps. (b) Depth profile of corrected CaKα maps. Color scales are as for Figure 1.

al., 2000]. We examine each of these potential sources of the observed Fe hot spots.

4.1.1. Atmospheric Dust Deposition as a Source of Fe Hot Spots

[15] The Total Ozone Mapping Spectrometer (TOMS) satellite, from which dust concentrations can be derived, was not operational during the time period leading up to our sample collection. Mineral dust records from the IMPROVE network of aerosol monitoring stations [*Eldred et al.*, 1990] did not show any major dust events to the subarctic Pacific prior to our sample collection (Figure 6). Field observations of dust enhancement of productivity in the subarctic Pacific in 2001 showed that the stimulating effects of the dust are transient, lasting only about 2 weeks [*Bishop et al.*, 2002]. This suggests that the bioavailable fraction of iron from dust is used up quickly, and argues against any lingering effects of dust deposited a long time before.

[16] We measured Ti:Fe ratios of individual hot spots as a tracer for Asian dust, which has a Ti:Fe of ∼0.1 [*VanCuren and Cahill*, 2002]. Of the 96 hot spots we analyzed in the 1- to 53-μm size fraction from the upper 100 m at Ocean Station Papa in February, only one had Ti:Fe as high as 0.1; the rest averaged ∼0.02 and matched closely the Ti:Fe value from the coastal station P4 (0.019) (Figure 7). Asian dust is therefore an unlikely source of our Fe hot spots.

4.1.2. Lateral Transport From the Continental Margin as a Source of Fe Hot Spots

[17] The subarctic Pacific exhibits a strong year-round horizontal pycnocline at about 150 m (Figure 8a) [*Bishop et al.*, 1999; *Whitney and Freeland*, 1999], which is also about the depth of the continental shelf surrounding the Gulf of Alaska in the northeast subarctic Pacific. Since transport generally occurs along constant density surfaces, this horizontal pycnocline may provide a ready connection from the continental shelf to the open ocean, as well as help to retain

iron in the upper ocean. Indeed, bulk acid leachable particulate Mn profiles along the coastal to open ocean transect all show a clear maximum at 150 m (Figure 8b). Particulate Mn is a known tracer for continental margin influences [*Bishop and Fleisher*, 1987], and the Mn profiles corroborate a continental margin signal propagating to OSP.

[18] The acid leachable particulate Fe also shows a maximum at the depth of the continental shelf at the coastal station (P4). The shape of the Fe maximum is broader than that for Mn, suggesting that there are additional deeper sources of Fe to the water column, likely wherever reducing sediments occur, such as the shelf break and upper continental slope. The propagation of the continental margin signal that is suggested by the Mn profiles is not as clear in bulk acid leachable Fe, however; while there is a maximum in acid leachable Fe at 150 m at Stations P4 and P16, it is not apparent at OSP (Figure 8c). Profiles of Fe hot spot concentration derived from synchrotron XRF quantification provide insight into the origin of Fe beyond what can be interpreted from bulk acid leachable concentrations. The profiles of Fe hot spots in the 1- to 53-μm and >53-μm size fractions at OSP have their maxima at or above the pycnocline (Figures 9a and 9b).

[19] Examination of the 1- to 51-μm Fe hot spot profile from 55°S, 170°W in the Southern Ocean provides further insight into the significance of the Fe hot spots. In contrast to the near-surface maximum in hot spot concentration at OSP in the subarctic Pacific, the 1- to 51-μm Fe hot spot profile from the Southern Ocean shows a strong and deep maximum at 900 m (Figure 9c). The closest continental feature to the Southern Ocean station is the Campbell Plateau southeast of New Zealand, spanning depths of 500–1000 m, and located about 650 km upstream of our station. The location of the maxima in Fe hot spot concentrations at the depths of continental features in two very
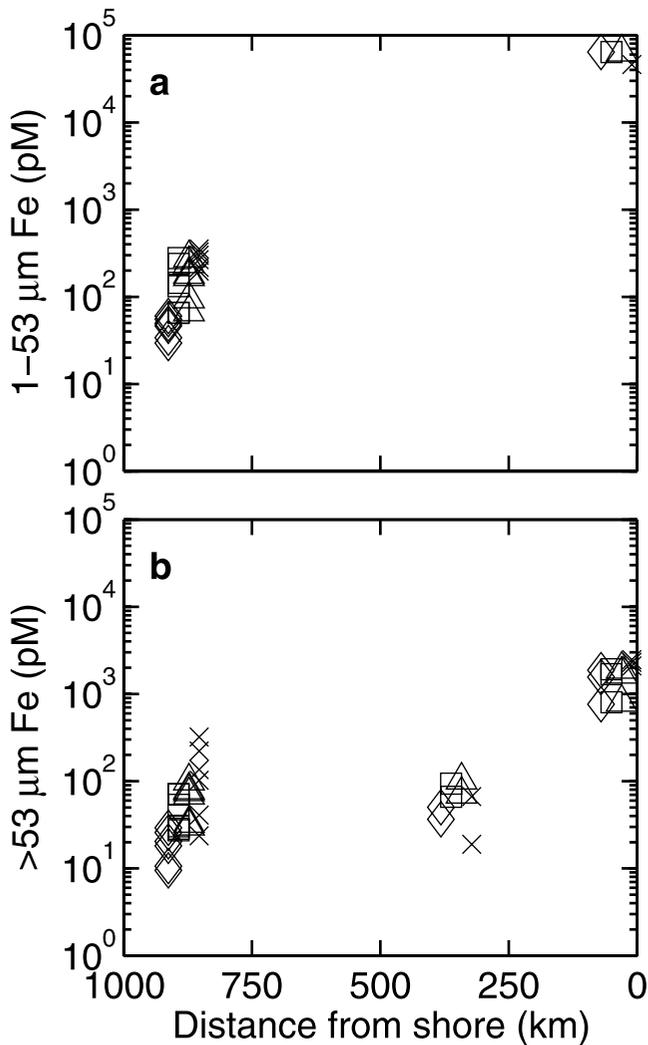
Figure 3. Lateral gradient of XRF- and inductively coupled plasma mass spectrometry (ICP-MS) determined Fe concentrations in the upper 200 m in the subarctic Pacific from Stations OSP, P16, and P4 (left to right) in (a) the 1- to 53-μm size fraction and (b) the >53-μm size fraction. No 1- to 53-μm samples from P16 were analyzed. Hot spot Fe (diamonds) is the sum of all Fe from pixels above the hot spot threshold, defined as 10 times the detection limit; XRF Detectable Fe (squares) is the sum of all Fe from pixels above the detection limit; total XRF Fe (triangles) is the sum of corrected Fe over the entire map; ICP-MS Fe (crosses) is the acid leachable Fe determined by ICP-MS. Symbols for the different types of Fe are offset from each other by 40 km for better visual clarity. Actual distance from shore is plotted for triangles.

different ocean basins strongly suggests that Fe hot spots are a marker for continental iron that was transported laterally from the continental shelf.

[20] The observation that there is no corresponding deep maximum in the >51-μm size fraction at 55°S (Figure 9d) suggests the mechanism by which Fe hot spots are transported and incorporated into >53-μm aggregates. Aggregates are formed when small particles such as phytoplankton

flocculate or are packaged into fecal matter after being grazed by zooplankton. The micron-sized Fe particles that show up as hot spots likely originate in the reducing sediments of the continental margin. They are transported by ocean circulation over long distances as micron-sized particulate iron (mostly Fe hydroxides), and are transferred to the large size fraction (>53 μm) only when passively captured by aggregating particles. In the 55°S samples, the source of the micron-sized Fe particles was likely the deep (500–1000 m) Campbell Plateau. The particle concentration is very low at this depth since it is well below the euphotic zone where phytoplankton grow. As a result, there is little aggregation activity and Fe hot spots from the originating small size fraction (1–51 μm) are not transferred into the large size fraction (>51 μm). The relatively high Fe hot spot concentrations in the >51-μm size fraction at 15 m and 138 m at 55°S were not associated with aggregates and may thus be due to contamination.

4.1.3. Upwelling as a Source of Fe Hot Spots

[21] Finally, if upwelling of Fe-rich deep waters were the source of Fe hot spots at OSP, we would expect the concentration of hot spots to increase with depth. Since there is a surface maximum in hot spot concentration at OSP and a decrease with depth, upwelling is unlikely to be the source.

4.2. Fe Transport From the Continental Margin

[22] Having eliminated atmospheric dust deposition and upwelling as sources of the Fe hot spots, we use an ocean general circulation model to examine the plausibility of particulate iron transport from the continental margin in the subarctic Pacific. We ran the ocean component (the Parallel Ocean Program, POP) of the Community Climate System Model version 2.0.1 (CCSM2, www.ccsm.ucar.edu/models/ccsm2.0.1) with passive "data" versions of the atmosphere, land, and ice components. The ocean model is forced using monthly averaged climatological wind stresses, heat fluxes, and freshwater fluxes from a previous integration of the fully active coupled CCSM2. The resolution of the model is relatively coarse (∼1° in the North Pacific), but it includes parameterizations for eddy-induced mixing.

[23] We added a hypothetical inert particulate tracer to the model whose source was a constant unit flux from the continental margin surrounding the Gulf of Alaska down to 200 m (Figure 10). This source was spread throughout the water column above 200 m to account for a sloping shelf. We simulate the loss of this tracer from gravitational settling by assigning low and high sinking velocities (10^{-4} and 10^{-3} cm/s) to the tracers. These represent the Stokes' sinking velocities of spherical iron hydroxide-like particles with diameters of 1 and 3 μm, respectively, which are reasonable given the size and composition of our iron-rich particles.

[24] The concentration of tracer at any grid point is described by the tracer tendency equation, and is a result of transport from horizontal advection and eddy mixing, transport from vertical advection, sinking, and diffusion, and an internal source term that is zero away from the margin source region. We do not simulate the transfer to and subsequent removal of tracer due to quickly settling large
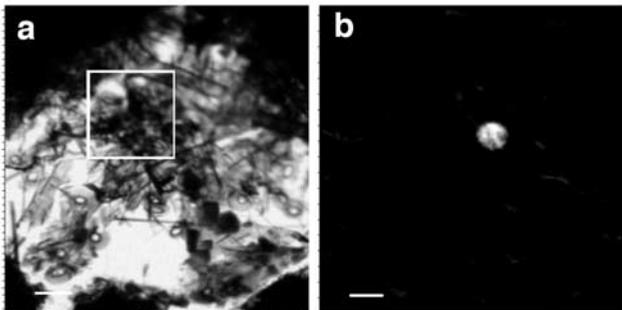
Figure 4. Scanning transmission X-ray microscope images of a thin aggregate from a 46-m >53-μm OSP sample from February 1996. (a) Image taken at 710 eV (above the Fe L$_3$-edge) showing diatom fragments (long spines) and coccoliths (round plates); scale bar = 5 μm. (b) Fe-specific image (image above the Fe L$_3$-edge (710 eV) minus image below the Fe L$_3$-edge (704 eV)) of outlined area from Figure 4a, showing a single Fe-rich particle of diameter ∼0.8 μm; scale bar = 1 μm.

aggregates. The model thus represents an upper limit of tracer concentration. Further model details are in the auxiliary material.

[25] The tracer reaches OSP after 14 months. The tracer gradient in the model (Figure 10) is consistent with that observed in the transect (Figures 3 and 8). Further, the model shows that the shelf source for OSP is from the west, whereas the source for P16 and P4 is from the east (Figure 10). We had first hypothesized that the Canadian coast is the source of materials to OSP. However, Figure 10 shows a tracer minimum centered around 140°W between tracers from the shelf sources.

[26] We compare the relative magnitudes of the terms in the tracer tendency equation for points along Line P out to the Alaskan coast. At OSP and points to the west, the horizontal advection term of the tracer tendency equation dominates all other terms. At all points east of the tracer minimum, including stations P16 and P4, the only input of tracer is from horizontal eddy mixing. This suggests that iron at OSP is from advective transport from the Alaskan shelf, whereas iron at P16 and P4 is primarily due to horizontal eddy mixing from the Canadian shelf. A strong recirculation from the Aleutians back to OSP is consistent with drifter studies of circulation in the subarctic Pacific [*Bograd et al.*, 1999]. The importance of the horizontal eddy mixing term at P16 and P4 is consistent with observations of the offshore (westward) transport of major nutrients by mesoscale eddies in the northeast subarctic Pacific [*Whitney and Robert*, 2002]. The "3-μm" tracer settles out before reaching OSP.

[27] The Fe hot spots were observed in both February and May 1996 at OSP. Biological packaging and sinking of large aggregates have been shown to strip waters of micron-sized oxide particles within 2−3 months when isolated from the source of the oxides [*Bishop and Fleisher*, 1987]. The continued presence of hot spots in large (>53 μm) aggregates (residence time in the surface ocean of order days) in

both February and May 1996 at OSP, along with prevalent hot spots in the small (1−53 μm) size fraction, implies a strong and continual source of fine particulate iron from the continental margin.

4.3. Bioavailability of Fe From Continental Margin

[28] At OSP in February, we observed a phytoplankton bloom as well as an unusual biological assemblage typical of iron-rich waters. In the sections above, we argue for the continental margin origin of the Fe hot spots. We now address the issue of the bioavailability of the Fe from the continental margin.

[29] Despite much lower light levels in February, surface values of particulate organic carbon (POC) were similar in February and May 1996, and depth-integrated (to 100 m) POC values were about twice as high in February compared to May [*Bishop et al.*, 1999]. Mixed layer OSP waters in February 1996 had double the chl *a* stock [*Boyd and Harrison*, 1999; *Thibault et al.*, 1999] and fucoxanthin (a diatom pigment) [*Thibault et al.*, 1999] as May. Particulate Si concentrations in the large size fraction (>53 μm), representing large diatoms, were 0.22 μM in February, compared to only 0.07 μM in May and 0.11 μM in August 1996. February samples also had much more biomass in the large size fraction: approximately 35% of the total (>1 μm) POC was in the >53 μm size fraction in February, compared to only 8% in May [*Bishop et al.*, 1999].

[30] There was very high grazing activity by large zooplankton in February 1996, as indicated by the fivefold higher surface concentrations of *pyrophaeophorbide a*, a tracer of copepod fecal pellet production, in February compared to May [*Thibault et al.*, 1999]. Integrations of all February *phaeophorbides* to 100 m are approximately double May values, indicating that total grazing of all size classes was also higher in February.
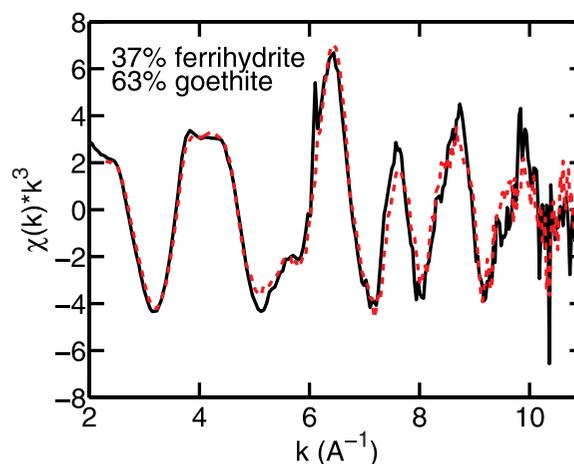

Figure 5. Extended X-ray absorption fine structure (EXAFS) data (black solid line) and least squares fit (red dashed line) of an iron hot spot from a 46-m >53-μm OSP sample from February. The EXAFS region was k^3 weighted. The data were fit with a linear combination of goethite (63%) and ferrihydrite (37%).

Table 2. Local Fe Bonding Environments in Hot Spots From Theoretical μ-EXAFS Fits[a]

Size Fraction	Hot Spot Identification	Backscatterer	μ-EXAFS Fit Parameters			
			CN	R, Å	σ^2	ΔE_0, eV
>53 μm	Julspot 1	O	4.6	2.01	0.011	-1.7
		Si	5.9	3.20	0.010	
>53 μm	Julspot 2	O	3.7	2.12	0.005	-1.0
		Fe	3.4	3.21	0.007	
		Si	2.1	3.18	0.001	
>53 μm	Julspot 7	O	3.1	1.96	0.001	-0.7
		O	2.3	2.16	0.000	
		Fe	3.7	2.97	0.012	
		Si	2.1	3.51	0.002	
>53 μm	Decspot 1	O	5.1	1.98	0.012	-1.7
		Fe	3.1	3.38	0.010	
		Fe	1.7	2.99	0.002	
		Fe	1.2	3.15	0.003	
>53 μm	Decspot 2	O	5.3	2.00	0.012	-1.3
		Fe	2.3	2.98	0.010	
		Fe	0.5	3.37	0.005	
		O	1.5	3.72	0.001	
>53 μm	Decspot 3	O	5.2	1.97	0.009	-1.8
		Fe	2.6	3.01	0.008	
		Fe	1.3	3.39	0.003	
		O	0.4	3.15	0.001	
1-53 μm	Sepspot 1	O	2.2	1.89	0.004	1.1
		O	2.9	2.04	0.001	
		Fe	3.2	3.05	0.004	
		Si	2.2	3.16	0.012	
1-53 μm	Sepspot 3	O	4.3	1.96	0.013	1.4
		Fe	1.5	3.41	0.003	
		Fe	1.2	3.00	0.004	
1-53 μm	Sepspot 5	O	3.0	1.93	0.007	0.1
		Fe	5.2	3.46	0.009	
		Fe	2.5	2.97	0.010	

[a]All Fe hot spots analyzed were from samples collected at 46 m from OSP in February 1996. The micro-extended X-ray absorption fine structure (μ-EXAFS) fit parameters are for absorber-backscatter pairs with Fe as the central absorber atom. CN is the coordination number; R is the interatomic distance from the Fe central absorption atom; σ^2 is the mean square relative displacement; ΔE_0 is the energy threshold difference; and χ^2 is the normalized error between the fit and smoothed EXAFS data.

[31] There was also evidence of export of particles out of the mixed layer. Surface waters in February showed a depletion of ^{234}Th [*Charette et al.*, 1999], indicating recent particle export. The chlorophyll flux at 100 m was at least 4 times higher in February than in May [*Thibault et al.*, 1999] (after ∼40% upward adjustment of the May values to account for differences in sediment trap depths using a Martin Curve: $F(z) = F_{100} (z/100)^{-0.858}$ [*Martin et al.*, 1987]). Unadjusted differences give a factor of 7. Similarly, depth-adjusted *pyrophaeophorbide a* flux was at least 3 times higher in February.

[32] The increase in chlorophyll stock, shift in size distribution, and prevalence of large diatoms are a strong indication of a recent supply of bioavailable iron in February [*Price et al.*, 1994; *Boyd et al.*, 1996]. The indications of enhanced grazing and export suggest that we sampled toward the end of a bloom in February. The Fe hot spots were also observed in May 1996 (Figure 2 and Table 1), yet the low chlorophyll and other biological parameters then were more characteristic of a typical iron-limited system. This argues that the Fe hot spots themselves are not very bioavailable. Although there is evidence that colloidal iron hydroxides can be used by mixotrophic phytoplankton in the North Pacific [*Maranger et al.*, 1998], it is still believed
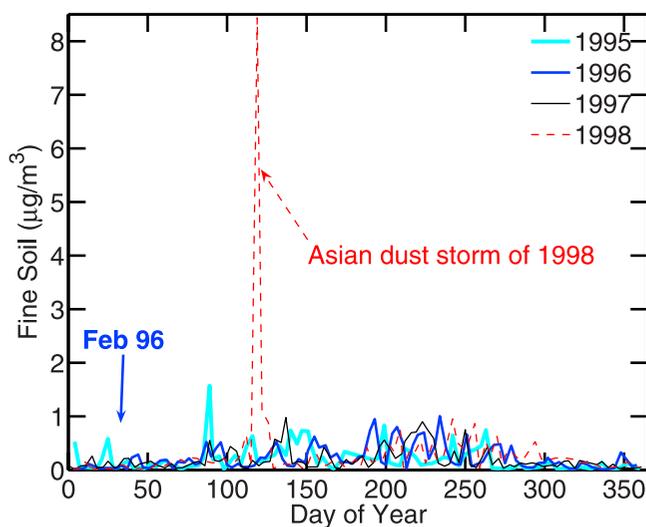

Figure 6. Mineral dust recorded at Mount Rainier National Park. Data are plotted for 1995–1998. No major dust events occured in the period preceding our sample collection at OSP (February 1996). Data are from the Interagency Program for Visual Environments (IMPROVE).
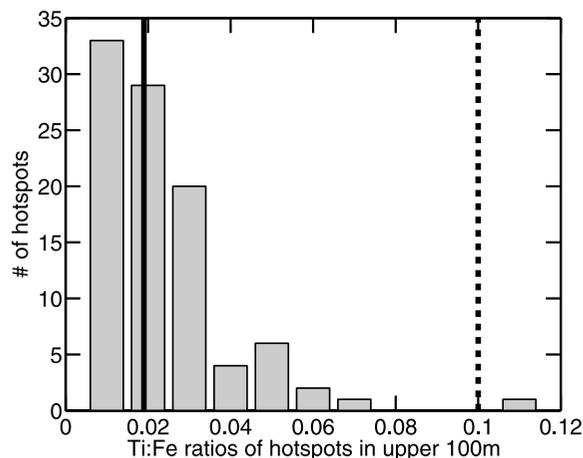
Figure 7. Histogram of Ti:Fe ratios of Fe hot spots in 1- to 53-μm samples from the upper 100 m at OSP in February 1996. Solid line shows Ti:Fe of Fe in coastal P4 samples. Dashed line shows Ti:Fe of Asian dust [*VanCuren and Cahill*, 2002; *VanCuren*, 2003].

that diatoms obtain iron from the dissolved phase only [*Nodwell and Price*, 2001].

4.4. Conceptual Framework for the Delivery of Fe From the Continental Margin

[33] We propose the following conceptual framework to explain the wintertime phytoplankton bloom at OSP. Reducing conditions within continental shelf and upper continental slope sediments result in remobilization of iron and the formation of oxyhydroxides in near bottom waters [*Johnson et al.*, 1999]. Previous studies have shown that the entrainment of particles from the continental shelf can be accompanied by high concentrations of dissolvable iron, as was found from the California coast [*Johnson et al.*, 1999; *Fitzwater et al.*, 2003], and the signal of dissolvable iron can be detected in surface waters 600 km offshore

[*Elrod et al.*, 2004]. The vertical cross section of tracer distribution from our model shows a component that is delivered from the Alaskan margin at the surface, as well as another that is delivered at 150 m (Figure 11). Here we emphasize the importance of the additional subsurface component of iron at 150 m that is transported from the continental margin along the pycnocline.

[34] The iron transported from the continental margin likely includes dissolved (bioavailable) and fine particulate (not strongly bioavailable) fractions. The dissolved bioavailable fraction in the surface component is likely consumed by coastal phytoplankton close to shore in all seasons. We propose that the subsurface component of bioavailable Fe has a more seasonal behavior. In the winter, low solar radiation means that the subsurface component of bioavailable Fe is below the base of the euphotic zone. Excess bioavailable iron from the continental margin in the subsurface component can thus survive the ∼1000-km journey to OSP. Deep mixing events from wintertime storms allow periodic access to this store of subsurface bioavailable Fe, bringing a new Fe supply to the euphotic zone. Access to a subsurface store of bioavailable Fe thus results in enhanced wintertime biological productivity in the open ocean, as we observed in February 1996 at OSP. In the springtime, the deeper penetration of light from increased solar radiation may allow deep phytoplankton to utilize the subsurface supply of bioavailable Fe. In addition, the mixed layer shoals and stratifies, which effectively isolates the phytoplankton in the mixed layer from the subsurface supply of Fe from the continental margin. As a result, the open ocean in the spring has a typical iron-limited phytoplankton assemblage, as we observed in May 1996 at OSP.

[35] The remaining nonbioavailable fine particulate fraction in both surface and subsurface components are advected out to the open ocean, regardless of season. Some fraction of this particulate material is captured into aggregates, where we observed them as iron hot spots within aggregates from the >53-μm size fraction.

[36] The wintertime iron source is thus a combination of an enhanced store of bioavailable iron in the subsurface in
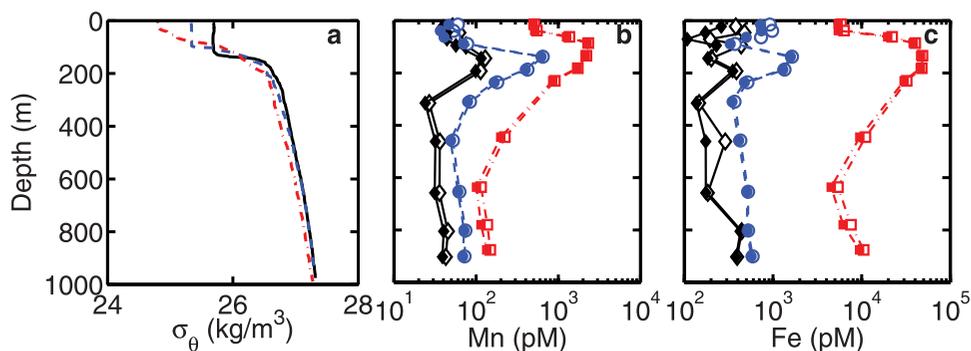

Figure 8. Depth profiles from an open ocean to coastal transect of (a) potential density in February 1996, (b) acid-leachable particulate Mn in February 1996 (OSP) and February 1997 (P16, P4), and (c) acid-leachable particulate Fe in February 1996 (OSP) and February 1997 (P16, P4). Solid symbols are for 1- to 53-μm size fraction; open symbols are total (>1 μm). Samples are from OSP (black solid line; diamonds), P16 (blue dashed line; circles), and P4 (red dash-dotted line; squares).
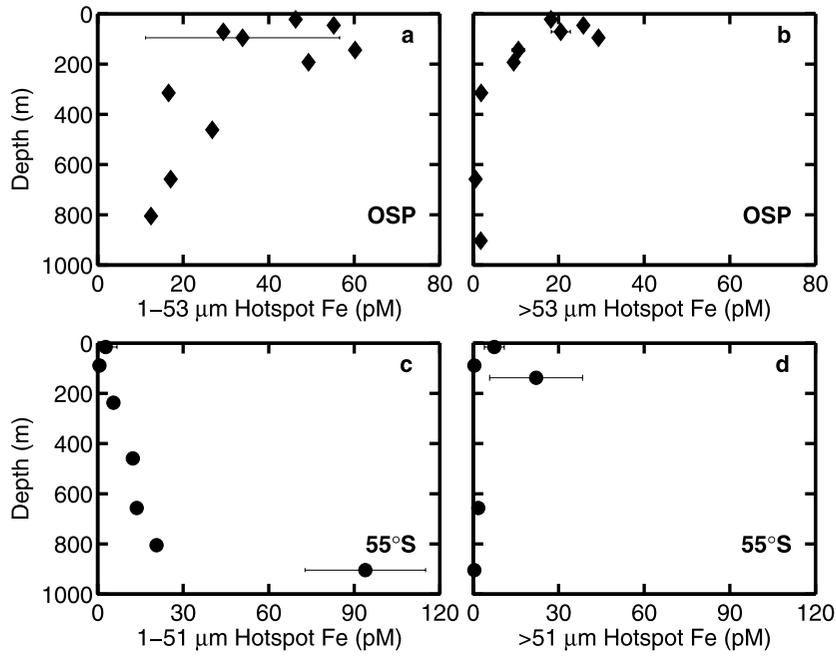
Figure 9. Profiles of Fe hot spot concentrations (a) in 1- to 53-μm size fraction at OSP in February 1996, (b) in >53-μm size fraction at OSP in February 1996, (c) in 1- to 51-μm size fraction at 55°S in the Southern Ocean in January 2002, and (d) in >51-μm size fraction at 55°S in the Southern Ocean in January 2002. Error bars are standard deviations for replicate samples.

the winter coupled with more frequent access to this store from deep-mixing wintertime storms.

[37] Periodic access to an additional supply of bioavailable Fe at OSP in the wintertime is supported by reports

Figure 10. Horizontal distribution of iron-like tracer concentrations in the northeast subarctic Pacific from an ocean general circulation model at the base of the model mixed layer (40 m). Station locations, shown as black crosses, are OSP, P16, and P4, from left to right. Tracer source regions are shown as gray dots. The model was run for 15 months. The tracer had a sinking velocity of 10^{-4} cm/s. Color bar shows the $\log_{10}$ of tracer concentrations in nanomoles per liter, assuming a 1 μmol/m^2/d source flux; contour intervals are 0.5 log units.

of higher dissolved Fe at OSP in February 1999 [*Nishioka et al.*, 2001], as well as previous iron addition experiments at OSP in February 1994 that showed no response to added iron, indicating that phytoplankton were not iron-limited at this time [*Boyd et al.*, 1995]. Iron addition experiments in February 1997 did show enhanced phytoplankton growth, however [*Maldonado et al.*, 1999]. We hypothesize that the waters for the February 1994 enrich-
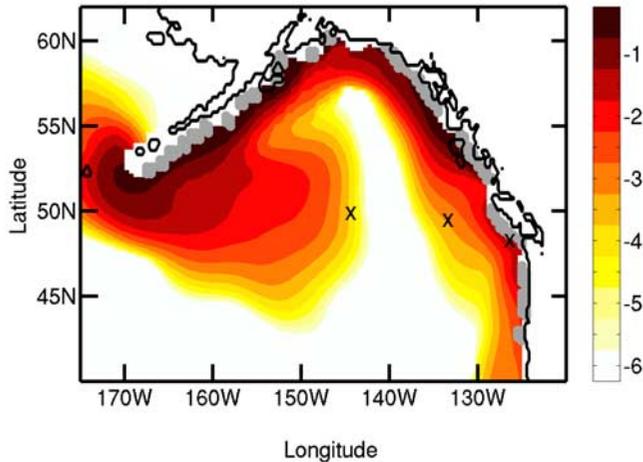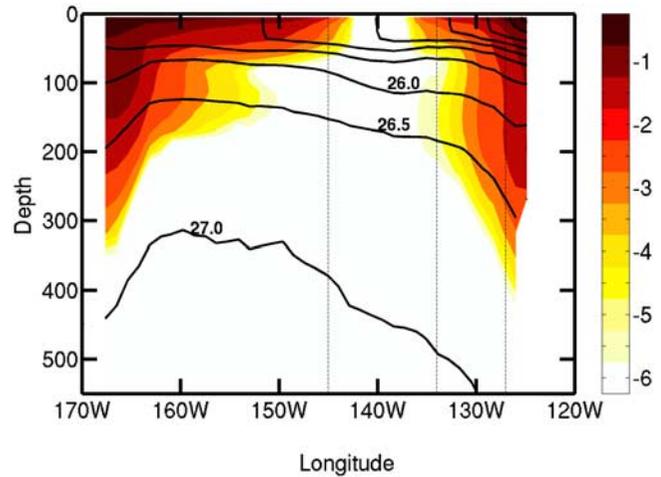

Figure 11. Cross section along line P showing vertical distribution of tracer. Tracer color bar is as for Figure 10. Thick black lines show horizontal isopycnal surfaces (σ_θ, kg/m^3); contour intervals are 0.5 kg/m^3. Dashed lines show station locations.

ment experiment that showed no response [*Boyd et al.*, 1995], our February 1996 samples, and the high dissolved Fe in February 1999 [*Nishioka et al.*, 2001] were sampled after deep mixing events that brought dissolved iron into the euphotic zone, and that the February 1997 enrichment experiment [*Maldonado et al.*, 1999] was conducted after a quiescent stretch that allowed the redevelopment of iron-limited conditions at OSP.

[38] The presence of Fe hot spots is thus a marker for the delivery of both particulate and dissolved bioavailable iron from the continental margin at 150 m. The small micron-sized particulates have a long residence time with respect to gravitational settling, and can be transported great distances to the middle of the open ocean. The dissolved bioavailable iron would likely be used in biological production, under favorable light and nutrient conditions. How much bioavailable iron arrives at OSP is thus dependent on productivity between the shelf and OSP. In February, the observed biological assemblage at OSP suggests that productivity along the delivery path is low because the low light does not penetrate to the pycnocline, and there is excess bioavailable iron arriving with the hot spots.

5. Conclusions

[39] Our analysis of iron hot spots and the winter bloom at OSP provide the first evidence of the delivery and importance of iron from the continental margin and its arrival at OSP in the open HNLC subarctic Pacific. We thus add the iron-limited subarctic Pacific to the growing list of open ocean regions, including the oligotrophic North Pacific [*Johnson et al.*, 2003] and the Atlantic sector of the Southern Ocean [*de Baar et al.*, 1995], that appear to be receiving iron from the continental margin.

[40] The subarctic Pacific is one of the three major iron-limited regions of the oceans [*Boyd et al.*, 2004]. Mesoscale and bottle iron enrichment experiments have demonstrated iron limitation in summer [*Boyd et al.*, 1996, 2004]. Recent observations of biomass stimulation in the subarctic Pacific by an Asian dust storm in April have confirmed that dust can relieve Fe limitation at OSP in spring [*Bishop et al.*, 2002]. We suggest that the entire continental shelf from California to the Aleutian Islands may be a source of additional iron in winter to the North Pacific. The degree of iron limitation in the subarctic Pacific is therefore not constant through the year and productivity can be boosted by different natural iron sources in different seasons.

[41] Phytoplankton compensate for low light levels by increasing cellular iron demand [*Maldonado et al.*, 1999]. The wintertime delivery of bioavailable iron to the subarctic Pacific may address the paradox of why wintertime chlorophyll levels in subpolar HNLC regions are so high despite light limitation [*Banse*, 1996; *Banse and English*, 1999]. We postulate that subsurface delivery of bioavailable iron from continental shelves and deep wintertime mixing allow for the higher than expected levels of productivity in subpolar HNLC regions by directly relieving iron limitation and partially relieving light limitation.

[42] A shelf iron source was incorporated into the most recent iron-ecosystem model [*Moore et al.*, 2004], but its effects were found to be limited to coastal regions because the sedimentary iron was quickly scavenged out of the water column. As a result, the sensitivity of global ocean primary production to the shelf iron source was low. Satellite studies of ocean color have shown that the island-mass effect on chlorophyll can persist for hundreds to a thousand kilometers offshore [*Moore and Abbott*, 2000], however, implying that shelf iron can have a longer-range effect than is currently represented in models. Our data and published ocean color satellite studies suggest that iron from shelf and continental sources is affecting the productivity of open ocean HNLC regions far (hundreds of kilometers) downstream, and that the current parameterizations for scavenging of iron in models may need to be modified to reflect the importance of this other source of iron.

References

Ankudinov, A. L., B. Ravel, J. J. Rehr, and S. D. Conradson (1998), Real space multiple scattering calculation of XANES, *Phys. Rev. B*, *58*(12), 7565–7576.

Archer, D. E., and K. Johnson (2000), A model of the iron cycle in the ocean, *Global Biogeochem. Cycles*, *14*(1), 269–279.

Atkinson, A., M. J. Whitehouse, J. Priddle, G. C. Cripps, P. Ward, and M. A. Brandon (2001), South Georgia, Antarctica: A productive, cold water, pelagic ecosystem, *Mar. Ecol. Prog. Ser.*, *216*, 279–308.

Aumont, O., E. Maier-Reimer, S. Blain, and P. Monfray (2003), An ecosystem model of the global ocean including Fe, Si, P colimitations, *Global Biogeochem. Cycles*, *17*(2), 1060, doi:10.1029/2001GB001745.

Banse, K. (1996), Low seasonality of low concentrations of surface chlorophyll in the Subantarctic water ring: Underwater irradiance, iron, or grazing?, *Prog. Oceanogr.*, *37*(3–4), 241–291.

Banse, K., and D. C. English (1999), Comparing phytoplankton seasonality in the eastern and western subarctic Pacific and the western Bering Sea, *Prog. Oceanogr.*, *43*(2–4), 235–288.

Bishop, J. K. B., and M. Q. Fleisher (1987), Particulate manganese dynamics in Gulf-stream warm-core rings and surrounding waters of the NW Atlantic, *Geochim. Cosmochim. Acta*, *51*(10), 2807–2825.

Bishop, J. K. B., D. Schupack, R. M. Sherrell, and M. Conte (1985), A multiple-unit large-volume in-situ filtration system for sampling oceanic particulate matter in mesoscale environments, in *Mapping Strategies in Chemical Oceanography*, *Adv. Chem. Ser.*, vol. 209, edited by A. Zirino, pp. 155–175, Am. Chem. Soc., Washington, D. C.

Bishop, J. K. B., S. E. Calvert, and M. Y. S. Soon (1999), Spatial and temporal variability of POC in the northeast subarctic Pacific, *Deep Sea Res., Part II*, *46*(11–12), 2699–2733.

Bishop, J. K. B., R. E. Davis, and J. T. Sherman (2002), Robotic observations of dust storm enhancement of carbon biomass in the North Pacific, *Science*, *298*(5594), 817–821.

Blain, S., et al. (2001), A biogeochemical study of the island mass effect in the context of the iron hypothesis: Kerguelen Islands, Southern Ocean, *Deep Sea Res., Part I*, *48*(1), 163–187.

Bograd, S. J., R. E. Thomson, A. B. Rabinovich, and P. H. LeBlond (1999), Near-surface circulation of the northeast Pacific Ocean derived from WOCE-SVP satellite-tracked drifters, *Deep Sea Res., Part II*, *46*(11–12), 2371–2403.

Boyd, P., and P. J. Harrison (1999), Phytoplankton dynamics in the NE subarctic Pacific, *Deep Sea Res., Part II*, *46*(11–12), 2405–2432.

Boyd, P. W., F. A. Whitney, P. J. Harrison, and C. S. Wong (1995), The NE subarctic Pacific in winter: 2. Biological rate processes, *Mar. Ecol. Prog. Ser.*, *128*, 25–34.

Boyd, P. W., D. L. Muggli, D. E. Varela, R. H. Goldblatt, R. Chretien, K. J. Orians, and P. J. Harrison (1996), In vitro iron enrichment experiments in the NE subarctic Pacific, *Mar. Ecol. Prog. Ser.*, *136*, 179–193.

Boyd, P. W., C. S. Wong, J. Merrill, F. Whitney, J. Snow, P. J. Harrison, and J. Gower (1998), Atmospheric iron supply and enhanced vertical carbon flux in the NE subarctic Pacific: Is there a connection?, *Global Biogeochem. Cycles*, *12*(3), 429–441.

Boyd, P. W., et al. (2000), A mesoscale phytoplankton bloom in the polar Southern Ocean stimulated by iron fertilization, *Nature*, *407*(6805), 695–702.

Boyd, P. W., et al. (2004), The decline and fate of an iron-induced subarctic phytoplankton bloom, *Nature*, *428*(6982), 549–553.

Charette, M. A., S. Bradley Moran, and J. K. B. Bishop (1999), 234Th as a tracer of particulate organic carbon export in the subarctic northeast Pacific Ocean, *Deep Sea Res., Part II*, *46*(11–12), 2833–2861.

Coale, K. H., S. E. Fitzwater, R. M. Gordon, K. S. Johnson, and R. T. Barber (1996), Control of community growth and export production by upwelled iron in the equatorial Pacific Ocean, *Nature*, *379*(6566), 621–624.

Coale, K. H., et al. (2004), Southern ocean iron enrichment experiment: Carbon cycling in high- and low-Si waters, *Science*, *304*(5669), 408–414.

de Baar, H. J. W., J. T. M. Dejong, D. C. E. Bakker, B. M. Loscher, C. Veth, U. Bathmann, and V. Smetacek (1995), Importance of iron for plankton blooms and carbon-dioxide drawdown in the Southern Ocean, *Nature*, *373*(6513), 412–415.

Eldred, R. A., T. A. Cahill, L. K. Wilkinson, P. J. Feeney, J. C. Chow, and W. C. Malm (1990), Measurement of fine particles and their chemical components in the NPS/IMPROVE Network, in *Transactions: Visibility and Fine Particles*, edited by C. V. Mathai, pp. 187–196, Air and Waste Manage. Assoc., Pittsburgh, Pa.

Elrod, V. A., W. M. Berelson, K. H. Coale, and K. S. Johnson (2004), The flux of iron from continental shelf sediments: A missing source for global budgets, *Geophys. Res. Lett.*, *31*, L12307, doi:10.1029/2004GL020216.

Fitzwater, S. E., K. S. Johnson, V. A. Elrod, J. P. Ryan, L. J. Coletti, S. J. Tanner, R. M. Gordon, and F. P. Chavez (2003), Iron, nutrient and phytoplankton biomass relationships in upwelled waters of the California coastal system, *Cont. Shelf Res.*, *23*(16), 1523–1544.

Fung, I. Y., S. K. Meyn, I. Tegen, S. C. Doney, J. G. John, and J. K. B. Bishop (2000), Iron supply and demand in the upper ocean, *Global Biogeochem. Cycles*, *14*(1), 281–295.

Gregg, W. W., P. Ginoux, P. S. Schopf, and N. W. Casey (2003), Phytoplankton and iron: Validation of a global three-dimensional ocean biogeochemical model, *Deep Sea Res., Part II*, *50*(22–26), 3143–3169.

Johnson, K. S., F. P. Chavez, and G. E. Friederich (1999), Continental-shelf sediment as a primary source of iron for coastal phytoplankton, *Nature*, *398*(6729), 697–700.

Johnson, K. S., et al. (2003), Surface ocean–lower atmosphere interactions in the Northeast Pacific Ocean Gyre: Aerosols, iron, and the ecosystem response, *Global Biogeochem. Cycles*, *17*(2), 1063, doi:10.1029/2002GB002004.

Kilcoyne, A. L. D., et al. (2003), Interferometer-controlled scanning transmission X-ray microscopes at the Advanced Light Source, *J. Synchrotron Radiat.*, *10*, 125–136.

Lefevre, N., and A. J. Watson (1999), Modeling the geochemical cycle of iron in the oceans and its impact on atmospheric CO_2 concentrations, *Global Biogeochem. Cycles*, *13*(3), 727–736.

Lindley, S. T., and R. T. Barber (1998), Phytoplankton response to natural and experimental iron addition, *Deep Sea Res., Part II*, *45*(6), 1135–1150.

Maldonado, M. T., P. W. Boyd, P. J. Harrison, and N. M. Price (1999), Co-limitation of phytoplankton growth by light and Fe during winter in the NE subarctic Pacific Ocean, *Deep Sea Res., Part II*, *46*(11–12), 2475–2485.

Maranger, R., D. F. Bird, and N. M. Price (1998), Iron acquisition by photosynthetic marine phytoplankton from ingested bacteria, *Nature*, *396*(6708), 248–251.

Marcus, M. A., A. A. MacDowell, R. Celestre, A. Manceau, T. Miller, H. A. Padmore, and R. E. Sublett (2004), Beamline 10.3.2 at ALS: A hard X-ray microprobe for environmental and materials sciences, *J. Synchrotron Radiat.*, *11*, 239–247.

Martin, J. H. (1991), Iron still comes from above, *Nature*, *353*(6340), 123.

Martin, J. H., G. A. Knauer, D. M. Karl, and W. W. Broenkow (1987), Vertex-carbon cycling in the northeast Pacific, *Deep Sea Res., Part A*, *34*(2), 267–285.

Martin, J. H., et al. (1994), Testing the iron hypothesis in ecosystems of the equatorial Pacific Ocean, *Nature*, *371*(6493), 123–129.

Moore, J. K., and M. R. Abbott (2000), Phytoplankton chlorophyll distributions and primary production in the Southern Ocean, *J. Geophys. Res.*, *105*(C12), 28,709–28,722.

Moore, J. K., S. C. Doney, and K. Lindsay (2004), Upper ocean ecosystem dynamics and iron cycling in a global three-dimensional model, *Global Biogeochem. Cycles*, *18*, GB4028, doi:10.1029/2004GB002220.

Nishioka, J., S. Takeda, C. S. Wong, and W. K. Johnson (2001), Size-fractionated iron concentrations in the northeast Pacific Ocean: Distribution of soluble and small colloidal iron, *Mar. Chem.*, *74*(2–3), 157–179.

Nodwell, L. M., and N. M. Price (2001), Direct use of inorganic colloidal iron by marine mixotrophic phytoplankton, *Limnol. Oceanogr.*, *46*(4), 765–777.

Parekh, P., M. J. Follows, and E. Boyle (2004), Modeling the global ocean iron cycle, *Global Biogeochem. Cycles*, *18*, GB1002, doi:10.1029/2003GB002061.

Perissinotto, R., R. K. Laubscher, and C. D. McQuaid (1992), Marine productivity enhancement around Bouvet and the South Sandwich Islands (Southern Ocean), *Mar. Ecol. Prog. Ser.*, *88*, 41–53.

Price, N. M., B. A. Ahner, and F. M. M. Morel (1994), The equatorial Pacific Ocean—Grazer-controlled phytoplankton populations in an iron-limited ecosystem, *Limnol. Oceanogr.*, *39*(3), 520–534.

Thibault, D., S. Roy, C. S. Wong, and J. K. Bishop (1999), The downward flux of biogenic material in the NE subarctic Pacific: Importance of algal sinking and mesozooplankton herbivory, *Deep Sea Res., Part II*, *46*(11–12), 2669–2697.

Tsuda, A., et al. (2003), A mesoscale iron enrichment in the western subarctic Pacific induces a large centric diatom bloom, *Science*, *300*(5621), 958–961.

VanCuren, R. A. (2003), Asian aerosols in North America: Extracting the chemical composition and mass concentration of the Asian continental aerosol plume from long-term aerosol records in the western United States, *J. Geophys. Res.*, *108*(D20), 4716, doi:10.1029/2003JD003678.

VanCuren, R. A., and T. A. Cahill (2002), Asian aerosols in North America: Frequency and concentration of fine dust, *J. Geophys. Res.*, *107*(D24), 4804, doi:10.1029/2002JD002204.

Whitney, F. A., and H. J. Freeland (1999), Variability in upper-ocean water properties in the NE Pacific Ocean, *Deep Sea Res., Part II*, *46*(11–12), 2351–2370.

Whitney, F., and M. Robert (2002), Structure of Haida eddies and their transport of nutrient from coastal margins into the NE Pacific Ocean, *J. Oceanogr.*, *58*(5), 715–723.

─────────────────

J. K. B. Bishop and G. A. Waychunas, Earth Sciences Division, Lawrence Berkeley National Laboratory, 1 Cyclotron Road, Berkeley, CA 94720, USA.

I. Y. Fung and C. C. Henning, Berkeley Atmospheric Sciences Center, University of California, Berkeley, Berkeley, CA 94720, USA.

P. J. Lam, Department of Marine Chemistry and Geochemistry, Woods Hole Oceanographic Institution, Woods Hole, MA 02543, USA. (pjlam@whoi.edu)

M. A. Marcus, Advanced Light Source, Lawrence Berkeley National Laboratory, 1 Cyclotron Road, Berkeley, CA 94720, USA.